Finer-Grained Image Splicing Localization Method Based on Noise Level Estimation

XiaoFeng Wang
School of science
Xi'an University of Technology
Xi'an, Shaanxi
xfwang66@sina.com.cn

ChunTao Jiang
School of science
Xi'an University of Technology
Xi'an, Shaanxi
tzmath@126.com

Qian Zhang
School of science
Xi'an University of Technology
Xi'an, Shaanxi
zq3_22@sina.com.cn

ABSTRACT
Digital image forensics is one of the important technologies to protect image content security, which aims to reveal malicious tampering in digital images. In this work, we propose a finer-grained image splicing localization method based on noise level estimation. In the proposed method, we extract statistical feature from the DCT coefficients of image, use such feature to estimate the noise of kurtosis statistic and feature of principal component. On the other hand, we estimate local noise using Laplace operator. The forensics features are formed by combining the kurtosis statistics noise, local Laplace noise, and the principal component feature. Then we use fuzzy C-means clustering to recognize suspect image blocks, and use a method of region marking to realize the finer-grained partition for regions. The spliced regions are detected according to the area ratio of image regions. Experimental results show that the proposed method has higher detection accuracy and stronger robustness.

CCS Concepts
Security and privacy → Multi-factor authentication

Keywords
Finer-grained image splicing localization; Image noise estimation; Fuzzy c-means clustering; Region marking.

1. INTRODUCTION
As the wide using of powerful image editing tools and image processing software, it is ubiquitous to alter the content of digital images without leaving any visible clues [1]. The existence of these fake images has caused serious problem even lead to crimes in many fields. As a key technology to protect the authenticity and integrity of image content, image tampering detection has become a research hotspot in academia and industry in recent years [2].

Image splicing tampering is one of the most common methods of image content attack. Image splicing detection has attracted great attention and received extensive research. Image splicing detection technologies are usually based on the assumption that image splicing/compositing will change the underlying pattern of the image and cause inconsistencies in image. Many earlier detection approaches aim to simply infer whether an image is a spliced image [3, 4, 5], but the locations of the tampering regions cannot be detected. Such methods usually regard image tampering detection as a problem of classification, and often achieve a high success rate. However, splicing regions localization have been the great challenge in this field.

In recent years, many scholars have devoted themselves to research the method of image splicing localization. Farid described a technique [6] to expose JPEG ghosts by detecting whether a part of an image was initially compressed at a lower quality than the rest of the image. Zuo et al. [7] proposed a composite image detection method via defining block measure [1] factors including re-sampling and JPEG compression. Amerini et al. [8] presented a method to distinguish and localize single and double JPEG compression in portions of an image through the use of the first digit features of the Discrete cosine transform (DCT) coefficients. In 2018, Iakovidou et al. [9] proposed a method to determine image forgery in JPEG compressed images by locating grid alignment anomalies. When creating composite images, the operation of splicing/compositing will cause the illumination inconsistency in image. Based on this property, Liu et al. [10] reported a detection method that is based on photometric consistency of illumination in shadows. Since image splicing may destroy the correlation introduced in Color Filter Array (CFA) interpolation, therefore, the inconsistency of CFA interpolation pattern can be used as the clue to reveal digital forgery. The most classic method was proposed by Popescu and Farid [11]. In their work, authors used the expectation maximization and linear model to detect and locate spliced image. Blurring is a common phenomenon in images, so the inconsistencies in motion blurring can be used to detect image regions from different sources. In [12], a splicing detection method based on local fuzzy type inconsistency was proposed. In this method, local fuzzy type detection features extracted from the estimated local fuzzy kernel are used to classify the image blocks into out-of-focus fuzzy or motion fuzzy, so as to generate a region with invariant fuzzy type.

Most digital images contain noises introduced during acquisition or subsequent processing. For natural images that have not been tampered with, the noise level is basically consistent in whole image. However, splicing regions from different sources may have different noise levels, and this inconsistency can be taken as evidence of image tampering. Mahdian et al. [13] proposed an image splicing detection method based on local noise inconsistency. Based on observation of kurtosis statistics in the band pass domain [14], Lyu et al. [15] proposed a splicing detection method based on blind local noise variance estimation. This method is not suitable for relatively complex noise models, and the noise variance may not be close enough for different intensification of untampered photos. Zhan et al. [16] estimated the local noise variance through Principal Component Analysis

ICMIP 2020, January 10–12, 2020, Nanjing, China

ACM ISBN 978-1-4503-7664-8/20/01…$15.00
https://doi.org/10.1145/3381271.3381274

Chuntao Jiang, Xiaofeng Wang, Qian Zhang are with the Xi'an University of Technology, Xi'an, Shaanxi, 710048, P.R.China.
Corresponding author: Xiaofeng Wang, E-mail: xfwang66@sina.com.cn

(PCA). This method can detect the tampering regions effectively. Zeng et al. [17] proposed an image splicing localization method by using PCA-based noise level estimation algorithms. In their work, authors perform blockwise noise level estimation of a test image with PCA, and segment the tampered region from the original region by k-means clustering. Yao et al. [18] revealed the relationship between the Noise Level Function (NLF) and the camera response Function. They formulated a Bayesian maximum a posteriori (MAP) framework to optimize the NLF estimation. Liu et al. [19] proposed a multi-target splicing detection method, which revealed the relationship between image noise and pixel intensity and proved its effectiveness and robustness for multi-target splicing detection. Nan et al. [20] proposed an image splicing detection method based on the noise level function, which fitted a curve by using noise variance and the sharpness of each block, then use the distance comparison to determine the tampering regions.

In this paper, we propose a finer-grained image splicing localization method based on noise level estimation. The main contributions are as follows. (1) we extract a kind of statistical feature from DCT coefficients, this feature can be well used to estimate the noise of kurtosis statistics. (2) we propose a region marking method to realize the finer-grained partition for suspect image regions. The spliced region is detected according to the area ratio of image region.

2. THE PROPOSED METHOD

In this section, we describe the proposed method. The proposed method consists of five stages, including feature selection, local noise estimation, DCT-coefficients-based principal component features extraction, Fuzzy c-means (FCM) clustering and splicing region localization. Fig.1 shows the schematic diagram of the proposed method.

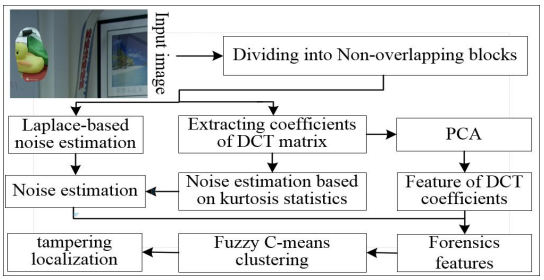

Figure 1. The schematic diagram of the proposed method.

2.1 Feature Selection

For image $I(x,y)$ of the size $W \times H$,

$$I(x,y) = I_0(x,y) + N(x,y) \quad (1)$$

Where $I_0(x,y)$ stands for the noise-free image and $N(x,y)$ represents a Gaussian noise. $I_0(x,y)$ and $N(x,y)$ are independent. We divide the image $I(x,y)$ into non-overlapping uniform blocks A_i with the size $a \times a$, where $i = 1,2,...,Q$, $Q = (W \times H)/(a \times a)$. Then each block is subjected to DCT transformation. Assume its DCT coefficient matrix is:

$$M_i = \begin{bmatrix} m_{11}^i & m_{12}^i & \cdots & m_{1a}^i \\ m_{21}^i & m_{22}^i & \cdots & m_{2a}^i \\ \vdots & \vdots & \ddots & \vdots \\ m_{a1}^i & m_{a2}^i & \cdots & m_{a\times a}^i \end{bmatrix} \quad (2)$$

In order to investigate the influence of different size of image blocks and different directions of DCT coefficients on the estimation of image noise level, we take 200 images randomly from the BSDS database. We process these images by adding zero mean Gaussian noise with the variance $\sigma = 3$, then divide these images into uniform non-overlapping blocks with the size $a \times a$, $(a = 9,17,25)$, respectively, and perform DCT transformation on each block to obtain the coefficient matrix. Then the values in different directions of the coefficient matrix are selected (as shown in Fig.2). We estimate the noise level of each block by using kurtosis statistic, respectively, and calculate the variance of the mean noise of all blocks, and the results are listed in Table 1.

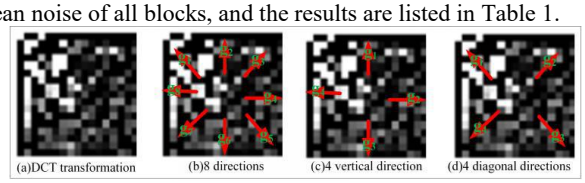

Figure 2. DCT coefficient feature selection method

As can be seen from the Table 1, when $a = 9$ and the DCT matrix coefficients of 4 vertical directions are taken, the estimated noise mean is 2.90, it is the closest to 3. This means that the noise estimate is relatively accurate. Therefore, it is reasonable to estimate noise using $a = 9$, and the DCT matrix coefficients of 4 vertical direction.For each image block A_i, the DCT coefficient features can be expressed as:

Table 1. Mean and variance of noise estimated using different sizes of image blocks and different directions of DCT coefficients

$a \times a$	25×25			17×17			9×9		
Direction selection	8	4(vertical)	4(diagonal)	8	4(vertical)	4(diagonal)	8	4(vertical)	4(diagonal)
Mean of noise variance	3.69	3.86	4.00	3.38	3.54	3.83	2.74	2.90	3.39
Variance of noise variance	0.76	1.11	0.66	0.65	0.89	0.62	0.53	0.71	0.64

$$g_{i1} = (m_{55}^i, m_{45}^i, m_{35}^i, m_{25}^i, m_{15}^i)$$
$$g_{i2} = (m_{55}^i, m_{56}^i, m_{57}^i, m_{58}^i, m_{59}^i)$$
$$g_{i3} = (m_{55}^i, m_{65}^i, m_{75}^i, m_{85}^i, m_{95}^i)$$
$$g_{i4} = (m_{55}^i, m_{54}^i, m_{53}^i, m_{52}^i, m_{51}^i)$$

$$\text{Let } G_i = (g_{i1}, g_{i2}, g_{i3}, g_{i4}) \quad (3)$$

Where $g_{ij}(j = 1,2,3,4)$ represents the DCT matrix coefficients extracted from different directions, m_{st}^i stands for the coefficients in the DCT matrix, as shown Fig.2(c).

2.2 Noise Level Estimation Based on Kurtosis Statistics

It is supposed that the frequency domain image $F(u,v)$ is obtained after DCT transformation of the image $I(x,y)$,

$$F(u,v) = M(u,v) + n(u,v)$$

Where $M(u,v)$ and $n(u,v)$ correspond to $I_0(x,y)$ and $N(x,y)$, respectively. $M(u,v)$ and $n(u,v)$ are independent, so the variance and kurtosis of $F(u,v)$ can be written as [21]:

$$\sigma^2(F) = \sigma^2(M) + \sigma^2(n) \quad (4)$$

$$k(F) = \frac{u_4(M) + u_4(n)}{\sigma^4(F)} = \frac{\sigma^4(M)}{\sigma^4(F)} k(M) + \frac{\sigma^4(n)}{\sigma^4(F)} k(n) \quad (5)$$

Where $k(M)$ indicates the kurtosis of the original image, $k(n)$ denotes the kurtosis of gaussian noise. Because the noise distribution $N(x,y)$ in the pixel domain is gaussian distribution, the noise distribution $n(u,v)$ in the frequency domain is also gaussian distribution according to the central limit theorem, $k(n) = 0$ can be obtained. From equations (4) and (5), we can get

$$k(F) = \frac{\sigma^4(M)}{\sigma^4(F)} k(M) = \left(\frac{\sigma^2(F) - \sigma^2(n)}{\sigma^2(F)}\right)^2 k(M) \quad (6)$$

Extracting the kurtosis noise of the feature vector G:

$$[k(M),\sigma^2(n)]=\arg\min_{k(M),\sigma^2(n)}\sum_{i=1}^{4}\left[\hat{k}^{1/2}(g_i)-\left(\frac{\hat{\sigma}^2(g_i)-\sigma^2(n)}{\hat{\sigma}^2(g_i)}\right)\times k^{1/2}(M)\right]^2 \quad (7)$$

Where $\hat{k}$ denotes the kurtosis of an image with noise, $\hat{\sigma}$ represents the variance of the image with noise. First, we deformed the above equation and constructed the function,

$$L(k^{1/2}(M),\sigma^2(n))=\sum_{i=1}^{4}\left[\hat{k}^{1/2}(g_i)-k^{1/2}(M)+\frac{\sigma^2(n)}{\hat{\sigma}^2(g_i)}\times k^{1/2}(M)\right]^2 \quad (8)$$

The gradient of $L(k^{1/2},\sigma^2)$ with regards to the two parameters are computed as:

$$\frac{\partial L}{\partial k^{1/2}}=2\sum_{i=1}^{4}\left[\hat{k}^{1/2}(g_i)-k^{1/2}(M)+\frac{\sigma^2(n)}{\hat{\sigma}^2(g_i)}\times k^{1/2}(M)\right]\left(\frac{\sigma^2(n)}{\hat{\sigma}^2(g_i)}-1\right) \quad (9)$$

$$\frac{\partial L}{\partial \sigma^2}=2\sum_{i=1}^{4}\left[\hat{k}^{1/2}(g_i)-k^{\frac{1}{2}}(M)+\frac{\sigma^2(n)}{\hat{\sigma}^2(g_i)}\times k^{1/2}(M)\right]\times\frac{k^{1/2}(M)}{\hat{\sigma}^2(g_i)} \quad (10)$$

Let equations (9) and (10) be equal to 0, we can obtain

$$k^{\frac{1}{2}}(M)=\frac{Z_1\times Z_2-Z_3\times Z_2}{Z_4-Z_2^2} \quad (11)$$

$$\sigma^2(n)=\frac{1}{Z_2}-\frac{1}{k^{1/2}(M)}\times\frac{Z_1}{Z_2} \quad (12)$$

Here, $Z_1=\frac{1}{4}\sum_{i=1}^{4}\hat{k}^{1/2}(g_i)$ $Z_2=\frac{1}{4}\sum_{i=1}^{4}1/\hat{\sigma}^2(g_i)$

$Z_3=\frac{1}{4}\sum_{i=1}^{4}\hat{k}^{1/2}(g_i)/\hat{\sigma}^2(g_i)$, $Z_4=\frac{1}{4}\sum_{i=1}^{4}1/\hat{\sigma}^4(g_i)$

So the estimated noise standard deviation is $\sigma(n)$. Again, image $I(x,y)$ is divided into non-overlapping blocks B_r of size $b\times b$, where $r=1,2,...,R$, $R=(W\times H)/(b\times b)$ (we take $b=18$ in the experiment). By performing the above operation on all blocks B_r (R is the total number of image blocks), the estimated noise value σ_r can be obtained. The kurtosis noise estimation is shown in Fig.3. The estimated values are normalized,

$$C_r=\frac{\sigma_r}{\max(\sigma_r)},\ r=1,2,...,R \quad (13)$$

We can get the normalized vector $C=(C_1,C_2,...,C_R)$.

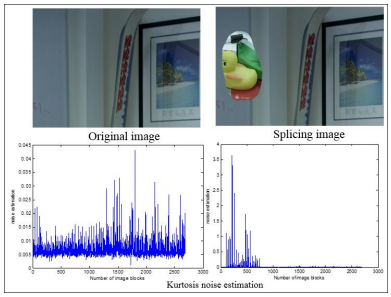

Figure 3. Estimation of kurtosis noise level.

2.3 Image Noise Estimation Base on Laplace Operator

According to the literature [22], image structures like edges have strong second order differential components, a noise estimator should be insensitive to the Laplacian L_1 and L_2 of an image.

$$L_1=\begin{bmatrix}0&1&0\\1&-4&1\\0&1&0\end{bmatrix}\quad L_2=\frac{1}{2}\begin{bmatrix}1&0&1\\0&-4&0\\1&0&1\end{bmatrix}$$

In order to estimate noise, A new Laplace operator L is constructed by using L_1 and L_2 ,as:

$$L=2(L_2-L_1)=\begin{bmatrix}1&-2&1\\-2&4&-2\\1&-2&1\end{bmatrix}$$

New mask L has zero mean and the same variance at each pixel. According to the work [22], noise variance $\hat{\sigma}_r$ of image block is

$$\hat{\sigma}_r=\sqrt{\frac{\pi}{2}}\frac{1}{6(b-2)(b-2)}\times\sum_{B_r}|B_r*L| \quad (14)$$

Normalization was carried out, as:

$$\hat{C}_r=\frac{\sigma_r}{\max(\sigma_r)},\ r=1,2,...,R$$

We can get the normalized vector $\hat{C}=(\hat{C}_1,\hat{C}_2,\cdots,\hat{C}_R)$ .For the obtained vectors $C=(C_1,C_2,...,C_R)$, $\hat{C}=(\hat{C}_1,\hat{C}_2,\cdots,\hat{C}_R)$,the following processing is performed to obtain a new noise estimate ω_r :

$$t=\max(\sigma_r)/\max(\hat{\sigma}_r)$$

$$\omega_r=\frac{C_r}{t}+\hat{C}_r \quad (15)$$

The estimated noise value of all image blocks is $\Omega=(\omega_1,\omega_2,...,\omega_R)$.

2.4 Principal Component Features of DCT Coefficient

As it has been proved in 2.1, using the image block size $a=9$, and four vertical directions of DCT coefficient matrix, the noise estimation is accurate. As a result, we subdivide each 18×18 image block into four image blocks $B_{rj}(j=1,2,3,4)$ with the size 9×9 , denoted as $B_r=(B_{r1},B_{r2},B_{r3},B_{r4})$ .We extracted the DCT matrix coefficient $G_{rj}(j=1,2,3,4)$ of each 9×9 image block B_{ri} :

$$G_{ri}=(g_{ri1},g_{ri2},g_{ri3},g_{ri4})$$

Then the DCT coefficient of 18×18 image blocks can be expressed as

$$G_r=\frac{1}{4}\sum_{j=1}^{4}G_{rj}$$

To extract the principal component of G_r , we use the algorithm of principal component analysis (PCA). Let

$$U_r=PCA(G_r) \quad (16)$$

Here, $PCA(\cdot)$ represents principal component analysis algorithm.

Then we use the mean of Ur to denote the information of the entire image block. The principal component features of DCT coefficient of each image block can be denoted as:

$$p_r=mean(U_r),r=1,2,\cdots,R \quad (17)$$

The principal component features of DCT coefficients of all image blocks can be denoted as $P=\{p_1,p_2,...,p_r\}$.

2.5 Splicing Region Localization

2.5.1 Detecting Spliced Image Region

Let $D=\{\Omega,P\}$, where Ω is noise standard deviation and P is the principal component feature of DCT coefficient. Using the FCM clustering algorithm, the dataset D is clustered into two categories. Fig.4 (b) shows the clustering result for image in Fig.4 (a). In Fig.4 (b), the red denotes splicing image regions, and the green indicates original image regions.

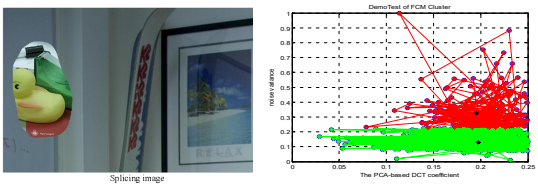

(a) (b)

Figure 4. The example of the Clustering results.

In general, we believe that the spliced image region should occupy smaller area in the image, so we define the image blocks that are included in the minority class as spliced regions.

Assuming that image blocks are divided into two categories, denotes as α and β. Let d_1, d_2 represent the number of image blocks in α and β, respectively, that is

$$\text{Let } d_1 = \|\alpha\|,\ d_2 = \|\beta\|$$

Here, $\|\bullet\|$ indicates the cardinality of a set. Then the suspect region F is defined as follows.

$$F = \begin{cases} \text{Regions consisting of image blocks contained in } \alpha, \text{if } d_1/(d_1+d_2) \le 0.5 \\ \text{Regions consisting of image blocks contained in } \beta, \text{others} \end{cases}$$

2.5.2 Finer-grained Tampering Localization for Splicing Region

To further refine detection results and obtain the precise location of the spliced regions, we perform following processing.

Step1: Secondary judgment for suspicious image blocks

We consider an image block as a suspicious block if it is surrounded by all suspicious blocks. For F_{uv}, if $F_{u+1,v}, F_{u-1,v}, F_{u,v+1}, F_{u,v-1} \in F$, then $F_{uv} \in F$, as shown in Fig.5.

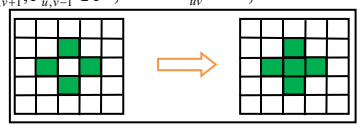

Figure 5. Secondary judgment for suspicious image blocks

Step2: Image region marking

The purpose of region marking is to mark suspicious image blocks as regions. As shown in Fig.6, we use red to denote pixels need to be marked. The first row has two regions with pixel positions of (3,5) and (7,9), respectively, they are marked as 1 and 2.

Then scan the second row, there are also two regions: (5), (7). Since they are adjacent to the two regions of the previous row, so we can use the region markers of the previous row, namely 1 and2.

There are two regions (2,3) and (5,7) in the third row. Since (5,7) is adjacent to the two regions in the previous row, the two previous regions are merged into one region and marked as the smallest of the two regions, namely 1. (2,3) has no adjacency to the previous row, so the new label 2 is given.

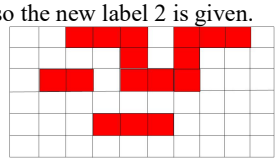

Figure 6. Image region.

The above process is carried out for the test image until all the pixels in all positions are marked, and each region is marked as $E_1, E_2 ... E_T$. T represents the total number of regions.

Step3: Calculate the area of each region and obtain the maximum area of these regions.

Let $S_1 = area(E_1),\ S_2 = area(E_2), \cdots, S_T = area(E_T)$ represent the area of each region $E_1, E_2 ... E_T$, respectively, let

$$E = \arg\max_{E_t}(S_1, S_2, \cdots, S_T), (t = 1,2...,T)$$

E is the spliced region.

3. EXPERIMENTAL RESULTS

3.1 Effectiveness

To test the effectiveness of the proposed algorithm, we first selected 20 images randomly from the BSDS200 database and created the splicing images manually. Then detect these images using the proposed method, the results are list in the Fig.7.

a b c d

Figure 7. Visual result of splicing detection.

In Fig.7, the first row presents the splicing images, and the second shows the detection result using the proposed method. The white region is the marked splicing region. As can be seen from the Fig.7, the visual effect of the splicing localization is satisfactory. In order to quantify analyze the performance of the proposed method, we consider the detection accuracy at the pixel level. To this end, the splicing pixels are regarded as positive sample and the original pixels as negative sample, and the true positive rates (TPR) and false positive rates (FPR) are used to evaluate the detection performance.

$$TPR = \frac{\text{The number of splicing pixels detected as splicing pixels}}{\text{The number of splicing pixels}} \times 100\%$$

$$FPR = \frac{\text{The number of original pixels detected as splicing pixels}}{\text{The number of original pixels}} \times 100\%$$

In order to more intuitively reflect the tamper locating performance of the above four images, we calculated the true and false positive rates and the results are listed in the Table 2.

Table 2. Pixel-level detection accuracy (%)

	a	b	c	d
TPR	100	97.8	100	97.7
FPR	0.03	2.01	0.03	1.09

From Table 2, it can be seen that the tamper detection ability and detection accuracy are more intuitive, and this method is proved to be effective.

3.2 Compared to Other Methods

In this section, we evaluate the detection accuracy of the proposed method by visual verification, and compare it with other relevant methods. To demonstrate the fairness of the experiment, we selected the public standard image library Columbia IPDED as the test data set. In the experiment, we used the proposed method and the method in [17] and [20] to detect the spliced images respectively. Fig.8 shows the splicing images and detection results in the Columbia IPDED.

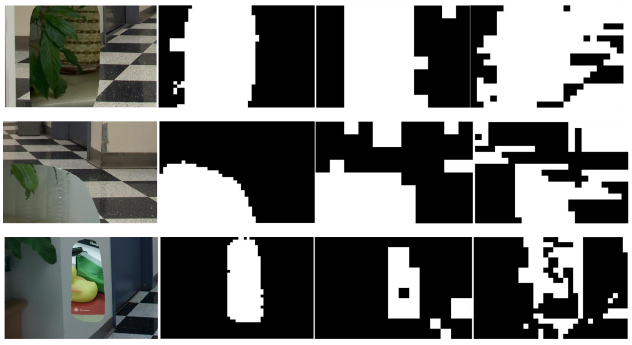

Figure 8. Splicing images and detection results.

In Fig 8, the images in the first column are spliced images from Columbia IPDED, the images in the second column are the detection results of the proposed method, and the image in the third and fourth columns are the detection results of work [17] [20] respectively. It can be seen from the Fig.8 that the method proposed in [17] can obtain the locating result, but the overall locating accuracy is not high and the false detection is large. Compared with [20], the proposed method has stronger tamper locating ability and lower false detection.

3.3 Robustness

Another important index to evaluate the performance of image splicing detection algorithm is its robustness. In this section, we evaluate the robustness of the proposed method via quantitative indicators, and compare with other related methods,see in Table 3.

Table 3. The average pixel-level detection accuracy on Columbia IPDED database

Method	(%)	No post-processing	JPEG compression			Down-sampling	Gamma correction	Gaussian blur(3×3)
			95	85	75	20%	Gamma=1	$\sigma=1$
Our method	TPR	72.2	65.9	61.3	56.2	62.2	62.1	63.2
	FPR	25.3	27.6	28.7	31.2	30.2	26.3	28.7
[17]	TPR	47.9	22.0	21.3	/	46	31.9	33.3
	FPR	18.5	10.8	11.7	/	23.5	17.4	19.7
[20]	TPR	67.3	64.5	62.2	61.9	60.3	62.4	61.5
	FPR	38.1	41.4	39.3	40.5	39.8	37.6	40.2

It can be seen from the Table 3 that our results are superior to the detection results of existing methods.

4. CONCLUSIONS

In this work, we propose a finer-grained image splicing localization method based on noise level estimation. The proposed method is different from the existing methods. In the proposed method, we extract a kind of statistical feature from DCT coefficients, this feature can be well used to estimate the noise of kurtosis statistics. We combine the local noise feature and the principal component feature to form forensics features. Then we use FCM clustering to recognize suspect blocks. In image splicing localization process, we propose a region marking method to realize the finer-grained partition for suspect image regions. The spliced region is detected according to the area ratio of image region.

5. ACKNOWLEDGMENT

This work was supported by the National Natural Science Foundation of China under Grant No.61772416; the Key Laboratory Project of the Education Department of Shaanxi Province under Grant No.17JS098; Shaanxi province technology innovation guiding project, No.2018XNCG-G-02.

6. REFERENCES

[1] Liu, G., Wang, J., Lian, S., Wang, Z. 2011. A passive image authentication scheme for detecting region-duplication forgery with rotation. Journal of Network and Computer Applications, 34(5), 1557-1565.

[2] Chang, S.F. 2007. Blind passive media forensics: motivation and opportunity. In International Workshop on Multimedia Content Analysis and Mining, Springer, Berlin, Heidelberg, 57-59.

[3] Zhang, Y., Zhao, C., Pi, Y. 2012. Revealing image splicing forgery using local binary patterns of DCT coefficients. In Communications, Signal Processing, and Systems, Springer, New York, NY, 181-189.

[4] Alahmadi, A. A., Hussain, M., Aboalsamh, H. 2013. Splicing image forgery detection based on DCT and Local Binary Pattern. In 2013 IEEE Global Conference on Signal and Information Processing, 253-256.

[5] Al-Hammadi, M. H., Muhammad, G., Hussain, M. 2013. Curvelet transform and local texture based image forgery detection. In International Symposium on Visual Computing, Springer, Berlin, Heidelberg, 503-512.

[6] Farid, H. 2009. Exposing digital forgeries from JPEG ghosts.IEEE transactions on information forensics and security,4(1),154-160.

[7] Zuo, J., Pan, S., Liu, B. 2011. Tampering detection for composite images based on re-sampling and JPEG compression. In the First Asian Conference on Pattern Recognition, IEEE, 169-173.

[8] Amerini, I, Becarelli, R., Caldelli, R. 2014 Splicing forgeries localization through the use of first digit features. In 2014 IEEE International Workshop on Information Forensics and Security (WIFS), IEEE, 143-148.

[9] Iakovidou, C., Zampoglou, M., Papadopoulos, S. 2018. Content-aware detection of JPEG grid inconsistencies for intuitive image forensics. Journal of Visual Communication and Image Representation,54, 155-170.

[10] Liu, Q., Cao, X., Deng, C..2011. Identifying image composites through shadow matte consistency. IEEE Transactions on Information Forensics and Security,6(3),1111-1122.

[11] Popescu, A. C., Farid, H. 2005. Exposing digital forgeries in color filter array interpolated images. IEEE Transactions on Signal Processing,53(10),3948-3959.

[12] Bahrami, K., Kot, A. C., Li, L. 2015. Blurred image splicing localization by exposing blur type inconsistency. IEEE Transactions on Information Forensics and Security,10(5),999-1009.

[13] Mahdian, B., Saic, S. 2009. Using noise inconsistencies for blind image forensics. Image and Vision Computing, 27(10):1497-1503.

[14] Lyu, S., Pan, X., Zhang, X. 2014. Exposing region splicing forgeries with blind local noise estimation. International journal of computer vision,110(2),202-221.

[15] Pan, X., Zhang, X., Lyu, S.2011. Exposing image forgery with blind noise estimation. In Proceedings of the thirteenth ACM multimedia workshop on Multimedia and security, pp 15-20.

[16] Zhan, L., Zhu, Y. 2015. Passive forensics for image splicing based on PCA noise estimation. In 2015 10th International Conference for Internet Technology and Secured Transactions (ICITST),IEEE, pp 78-83.

[17] Zeng, H., Zhan, Y., Kang, X.2017. Image splicing localization using PCA-based noise level estimation. Multimedia Tools and Applications, 76(4),4783-4799.

[18] Yao, H., Wang, S., Zhang, X., Qin, C. 2017. Detecting image splicing based on noise level inconsistency. Multimedia Tools and Applications, 76(10),12457-12479.

[19] Liu, B., Pun, C. M. 2017. Multi-object splicing forgery detection using noise level difference. In 2017 IEEE Conference on Dependable and Secure Computing,IEEE, 533-534.

[20] Zhu, N., Li, Z.2018. Blind image splicing detection via noise level function. Signal Processing: Image Communication, 68:181-192.

[21] Zhai, G., Wu, X. 2011. Noise estimation using statistics of natural images. In 2011 18th IEEE International Conference on Image Processing, 1857-1860.

[22] Immerkaer, J. 1996. Fast noise variance estimation. Computer vision and image understanding, 64(2),300-30.